www.elsevier.com/locate/jssc

Magnetic structures of β_I-Li_2CoSiO_4 and γ_0-Li_2MnSiO_4: Crystal structure type Vs. magnetic topology

Maxim Avdeev, Zakiah Mohamed, Chris D. Ling

PII: S0022-4596(14)00189-3
DOI: http://dx.doi.org/10.1016/j.jssc.2014.04.028
Reference: YJSSC18463

To appear in: *Journal of Solid State Chemistry*

Received date: 4 April 2014
Revised date: 27 April 2014
Accepted date: 29 April 2014

Cite this article as: Maxim Avdeev, Zakiah Mohamed, Chris D. Ling, Magnetic structures of β_I-Li_2CoSiO_4 and γ_0-Li_2MnSiO_4: Crystal structure type Vs. magnetic topology, *Journal of Solid State Chemistry,* http://dx.doi.org/10.1016/j.jssc.2014.04.028

Magnetic structures of β_I-Li_2CoSiO_4 and γ_0-Li_2MnSiO_4: crystal structure type vs. magnetic topology

Maxim Avdeev[‡,*], *Zakiah Mohamed*[†§], *Chris D. Ling*[†]

[‡] Bragg Institute, Australian Nuclear Science and Technology Organisation, Lucas Heights, NSW 2234, Australia

[†] School of Chemistry, The University of Sydney, Sydney, NSW 2006, Australia

[§] Faculty of Applied Sciences, Universiti Teknologi MARA, 40450 Shah Alam, Malaysia

KEYWORDS Neutron powder diffraction, magnetic structure, magnetic properties, lithium orthosilicate.

ABSTRACT: The magnetic structure and properties of the candidate lithium-ion battery cathode materials $Pbn2_1$(≡$Pna2_1$) Li_2CoSiO_4 and $P2_1/n$ Li_2MnSiO_4 have been studied experimentally using low-temperature neutron powder diffraction and magnetometry. Both materials undergo long-range antiferromagnetic ordering, at 14 K and 12 K respectively, due to super-super-exchange mediated by bridging silicate groups. Despite having different crystal structures (wurtzite- vs. "dipolar"-type), Li_2CoSiO_4 and Li_2MnSiO_4 have the same topology in terms of magnetic interactions, and adopt collinear magnetic structures of the same type with the propagation vectors (0,1/2,1/2) and (1/2,0,1/2), respectively. The magnetic moments in the two materials are aligned in parallel and obliquely to the distorted closed-packed layers of oxygen atoms. The experimentally observed values of the ordered magnetic moments, 2.9 μ_B and 4.6 μ_B, are close to those expected for d^7 Co^{2+} and d^5 Mn^{2+}, respectively.

---

[*] Corresponding author. Tel.: +61 02 9717 9522, fax: +61 02 9717 3606, email: max@ansto.gov.au

Introduction

Materials with the ratio $A:M^{+2} = 2:1$ ($A = Li^{+}$, Na^{+}; M = transition metal) draw a lot of attention in the field of battery research because they can – in theory – deliver up to two electrons *per* transition metal ([1] and references therein). The lithium orthosilicates Li_2MSiO_4 (M = Mn, Fe, Co, Ni) have attracted particularly strong interest recently, following the proposal of the Mn and Fe members as insertion cathode materials. [2] The crystal structures of the orthosilicates can be understood as being based on hexagonal close-packing of oxygen atoms in which half the tetrahedral voids are filled by Li, M, or Si. Different patterns of cation distribution over the tetrahedral positions and related structure distortions produce a large number of polymorphs, mostly with orthorhombic or monoclinic symmetry, which can be divided into two groups: those in which all the cation tetrahedra point in the same direction perpendicular to the oxygen close-packed layers; and those in which half of them point in the opposite direction (Figure 1). The two groups are commonly referred to in literature as "LT-Li_3PO_4"/"HT-Li_3PO_4"-type [3], β/γ-type [4], or "wurtzite"/"dipolar"-type [5], respectively. Within these groups, polymorphs with $P2_1$, $P2_1/n$, Pn, Pmnb, $Pmn2_1$, $Pbn2_1$ space group symmetries have been reported depending on the identity of M (Mn, Fe, or Co) and the synthesis conditions employed ([6, 7] and references therein), although more variations are theoretically possible [5].

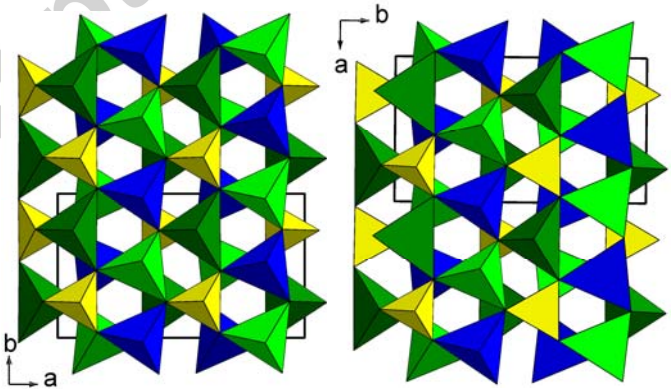

Figure 1. General view of Li_2MSiO_4 structure of "LT-Li_3PO_4" ≡ β ≡ "wurtzite"-type with all cation tetrahedra pointing in the same direction (left) and "HT-Li_3PO_4" ≡ γ ≡ "dipolar"-type with half of cation tetrahedra pointing in the opposite direction (right), perpendicular to close-packed oxygen layers. Blue, yellow, and light/dark green tetrahedra show the M, Si, and Li1/Li2 sites in $Pbn2_1$ Li_2CoSiO_4 and $P2_1/n$ Li_2MnSiO_4.

The crystal structure, temperature induced polymorphism, and electrochemical properties of orthosilicates have been thoroughly investigated by various research groups and later reviewed ([1] and references therein). However, despite this wide interest, data on some of the basic physical properties of orthosilicates remain very sparse. For example, magnetic properties have been investigated only for Li_2FeSiO_4 [8, 9] and Li_2MnSiO_4 [10] but not for Li_2CoSiO_4. Furthermore, while the Fe and Mn compounds were shown to order magnetically [8-10] (and Co might be expected to behave similarly), the magnetic structures have never been solved. Knowledge of the ordered magnetic ground states of these candidate lithium-ion battery cathode materials is motivated (beyond their fundamentally interesting magnetic topologies and structures) by the need to perform *ab initio* calculations with improved accuracy and correspondingly improved quantitative predictions of electronic and electrochemical properties. Numerous examples have shown that ignoring magnetic order in these materials results in large errors of both crystal structural parameters and predicted intercalation voltages (up to 30% for the latter, *eg*, [11, 12]).

In this work we report a detailed exploration of the magnetic structure and properties of $Pbn2_1$ Li_2CoSiO_4 and $P2_1/n$ Li_2MnSiO_4. We have found that despite belonging to the different (i.e., β and γ) structural families, these compounds share the same magnetic topology and thus adopt magnetic structures of the same type.

EXPERIMENTAL

Polycrystalline samples of Li_2CoSiO_4 and Li_2MnSiO_4 were prepared by conventional solid-state synthesis using Li_2CO_3, CoO, $MnCO_3$, and SiO_2 (Aldrich, all >99.9% purity).

For Li_2CoSiO_4, a stoichiometric mixture of the starting materials was ball-milled with ethyl alcohol for 5 h at 350 rpm. This mixture was heated in air at 400°C for 12 h and then at 600°C for 12 h. The sample was reground using a mortar and pestle before a final calcination at 1000°C for 5 h under flowing Ar gas. After the final heat treatment the sample was confirmed to be of the $Pbn2_1$ form. Although examination of X-ray powder diffraction (XRD) patterns revealed the presence of only one small impurity (Li_2SiO_3 [13]), more

sensitive magnetic measurements later indicated the presence of a ferromagnetic impurity in concentrations below the XRD detection limit (~1%) as discussed below.

For Li_2MnSiO_4, a stoichiometric mixture of starting materials was ball-milled for 3 h at 350 rpm in iso-propanol and dried overnight in air. The mixture was then sintered under Ar flow at 400°C for 4 h. The sample was reground, pelletized and calcined at 800°C and 1000°C for 24 h with intermediate regrinding and slowly cooled to room temperature. The collected XRD data showed, as expected, that the sample had taken the $P2_1/n$ form of Li_2MnSiO_4 [14]. Again, a small Li_2SiO_3 impurity was detected; neither XRD nor further magnetic measurements revealed any other impurity phases.

The temperature-dependent magnetization of the samples was measured using a Quantum Design Physical Properties Measurement System (PPMS) with a vibrating sample magnetometer (VSM) probe from 2 to 300 K in an applied magnetic field H = 50 kOe, under zero field-cooled (ZFC) and field-cooled (FC) conditions. Heat capacity measurements were performed for Li_2CoSiO_4 pellets made of powder samples in the vicinity of the magnetic transition.

Neutron powder diffraction data (NPD) were collected on the Echidna diffractometer at the OPAL reactor (Lucas Heights, Australia) using a neutron wavelength of 2.4395 Å. Rietveld analysis of the data was performed using the Fullprof Suite [15] with default neutron scattering lengths and Co^{+2} and Mn^{2+} magnetic form-factors.

RESULTS AND DISCUSSION

Magnetic properties

The results of magnetic property measurements for the two compositions are presented in Figure 2. The magnetic susceptibility χ_m as a function of temperature revealed a signature of antiferromagnetic (AFM) transitions at ~14 K and ~12 K for Li_2CoSiO_4 and Li_2MnSiO_4, respectively. Specific heat C_p measurements for Li_2CoSiO_4 showed a clear λ-type anomaly at ~14 K, confirming long-range magnetic ordering in agreement with the magnetic susceptibility measurement (Figure 2, inset). Additional measurements of magnetization as a function of magnetic field at 4 and 50 K revealed the presence of a ferromagnetic (FM)

impurity in the Li_2CoSiO_4 sample undetected by XRD. At both 4 K and 50 K (i.e., below and above the AFM transition) the sample demonstrated a nearly identical weak FM signal (Figure S1). The Li_2MnSiO_4 sample showed only a linear response as expected for an antiferromagnet (Figure S1).

Above ~150 K the magnetic susceptibility data obey a modified Curie-Weiss law $\chi_m = C(T - \theta) + \chi_0$ where χ_0 corrects for all temperature-independent contributions, C is the Curie constant and θ is the Curie-Weiss temperature. A linear fit over the range 200–300 K yielded $\theta = -23$ K, $\chi_0 = 0.0146$ emu/mol, and an effective magnetic moment, $\mu_{eff} = 4.3\ \mu_B$ for Li_2CoSiO_4; and $\theta = -38$ K, $\chi_0 = 0.00037$ emu/mol, and an effective magnetic moment, $\mu_{eff} = 5.7\ \mu_B$ for Li_2MnSiO_4. The negative θ values indicate predominantly AFM interactions in both materials. The effective moment for Li_2CoSiO_4 is typical for high-spin d^7 (S = 3/2) Co^{2+} with only partially quenched orbital moments ($\mu_{eff}^S = 3.9\ \mu_B$, $\mu_{eff}^{S+L} = 5.2\ \mu_B$), while that for Li_2MnSiO_4 is close to the value expected for high-spin d^5 (S = 5/2) Mn^{2+} ($\mu_{eff}^S = 5.9\ \mu_B$). ([16] and references therein)

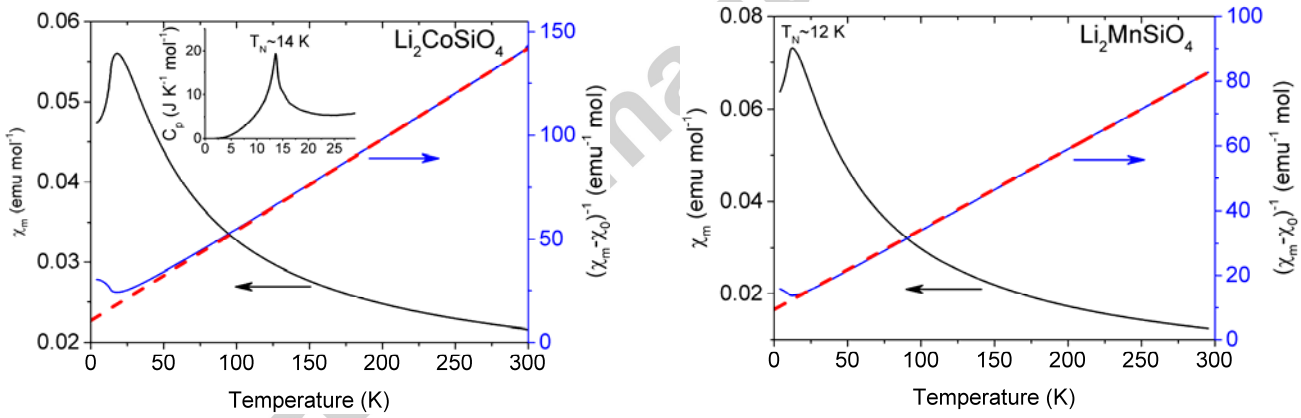

Figure 2. Magnetic susceptibility χ_m and $1/(\chi_m-\chi_0)$ as functions of temperature for $Pbn2_1$ Li_2CoSiO_4 (left) and $P2_1/n$ Li_2MnSiO_4 (right). The red lines show the linear fit to the modified Curie-Weiss equation. The inset shows heat capacity for Li_2CoSiO_4.

Crystal and magnetic structure

$Pbn2_1$ Li_2CoSiO_4

Neutron powder diffraction (NPD) data collected for Li_2CoSiO_4 at 20 K (i.e. above the transition temperature expected based on our magnetic susceptibility measurements), were successfully analyzed using the original structure model determined from X-ray single crystal diffraction data [17]. Given that a small degree of Li/Co anti-site disorder was reported more recently [18], this scenario was also tested. Although re-

finement indeed suggested some anti-site disorder (up to 3.9(8)% of Li at the Co site), the fit quality only improved from 5.90/6.35% to 5.88/6.28% in terms of R_p/R_{wp}, which can be considered as statistically insignificant. [19] We therefore used a fully ordered model for further magnetic structure analysis. We note, however, that the level of Li/Co disorder (if any) depends strongly on a synthesis protocol. As reported in Ref. [18], the Li/Co disorder decreases on increase of sample preparation temperature, from 2.4(16)% and 8.6(14)% for two metal sites in the Li_2CoSiO_4 sample prepared at 700°C to zero in the sample annealed at 1100°C [18]. This is consistent with the results of our NPD data analysis which yielded a statistically negligible level of the Li/Co disorder in the sample prepared in this study at 1000°C. The final Rietveld fit and crystallographic information for Li_2CoSiO_4 at 20 K are presented in Figure S2 and Table S1, respectively.

Examination of the NPD data collected at 3 K revealed additional diffraction peaks due to long-range magnetic ordering, in agreement with our magnetic susceptibility data. All the diffraction peaks with magnetic contributions could be indexed by the unit cell doubled along the *b* and *c* axes of the $Pna2_1$ unit cell (standard setting of $Pbn2_1$), i.e., with the propagation vector $k = (0,1/2,1/2)$. Representational analysis performed with BasIReps [15] for the Co(4a; x,y,z) site of the $Pna2_1$ space group revealed that this symmetry does not offer any reduction in the degrees of freedom for the magnetic structure; i.e., the magnetic moment components for all four Co atoms are independent (Table S2). We solved the magnetic structure using the simulated annealing technique (as implemented in Fullprof) with magnetic intensities extracted using the Le Bail profile matching method. Regardless of starting configuration, this process robustly produced the same solution, which was then further Rietveld-refined against the full NPD pattern assuming equal values for the magnetic moments on all Co atoms. The final Rietveld plot and crystallographic information are presented in Figure 3 and Table S3.

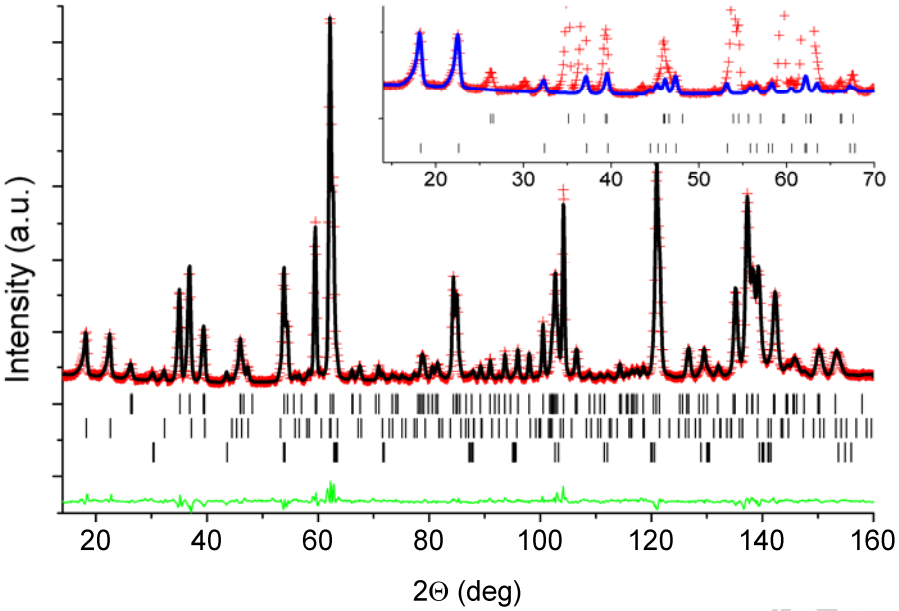

Figure 3. The Rietveld plot for Li_2CoSiO_4 refined against NPD data collected at 3 K. The red crosses and black and green solid lines indicate the observed and calculated patterns and their difference, respectively. The tick marks from top to bottom indicate the position of the diffraction peaks of the nuclear structure of Li_2CoSiO_4, the magnetic structure of Li_2CoSiO_4, and Li_2SiO_3, respectively. R_p = 2.71%, R_{wp} = 3.69%, $R_F(Li_2CoSiO_4)$ = 2.02%, R_{mag} = 7.42%. The blue curve in the inset shows the magnetic contribution only.

As expected from our susceptibility data, Li_2CoSiO_4 adopts an AFM structure (Figure 4), which we discuss in detail below in comparison to that of Li_2MnSiO_4. The magnetic moments are parallel to the *a* axis (of the $Pna2_1$ setting), i.e., they lie in the distorted layers of close-packed oxygen atoms. The refined value of the moment, 2.92(4) μ_B/Co, is close to that expected for S=3/2 d^7 Co^{2+}. The fact that the ordered moment is close to a spin-only value suggests quenching of the orbital moment contribution in the magnetically ordered state; the behaviour not unusual for Co^{2+} oxides ([20] and references therein).

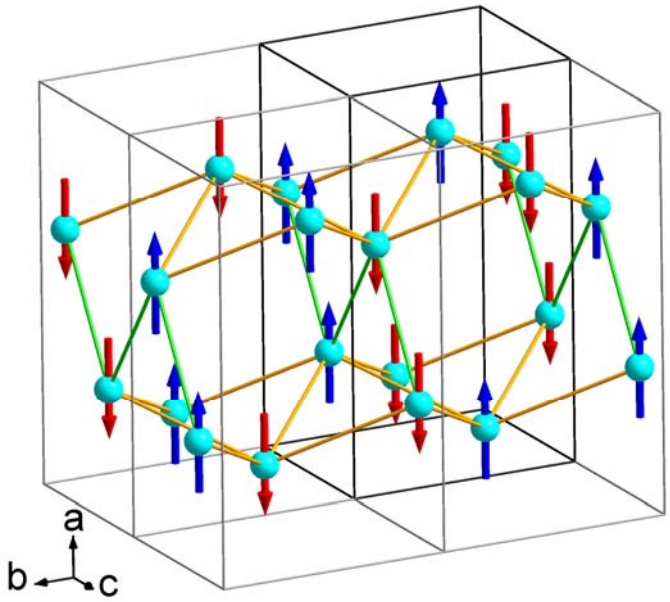

Figure 4. General view of the magnetic structure of Li_2CoSiO_4 in the $Pna2_1$ setting (non-magnetic atoms omitted). Nuclear and magnetic unit cells are shown with black and gray lines, respectively. Two sets of Co–Co distances (4.30 Å and 4.38 Å) are shown with green and yellow lines, respectively.

$P2_1/n$ Li_2MnSiO_4

NPD data collected for Li_2MnSiO_4 at 20 K, i.e., above the magnetic transition were successfully analysed using the original model determined using XRD data. [14] Since, as in the case of other orthosilicates, Li/Mn anti-site disorder could be expected, we first reviewed the relevant data published for the isostructural compositions. Although the results of previous studies show significant scatter, with the reported values varying from 0.7% to ~20% (Table S4), and disagree even on the type of the affected sites, Li/M anti-site mixing is a well-established fact. The only exceptions are the structures of Li_2ZnSiO_4 and Li_2MgSiO_4 (Table S4); however, the metal-mixing model does not seem to have been considered is those studies as pointed out in Ref. [14]. Therefore, the occupancies of all three metal sites ("Mn", "Li1", and "Li2") were refined under a constraint occ(Mn) + occ(Li) = 1. A non-negligible anti-site disorder was found only for the Mn and Li1 sites (9.8(1.8)% and 9.2(1.9)%, respectively). The fraction of Mn on the Li3 site converged to a slightly negative value (-0.01(1)) and was fixed to zero. This metal distribution is qualitatively similar to that found in a single crystal X-ray study of Li_2MgSiO_4 (Table S4), although again, M/Li mixing may be

expected to depend on how close the ionic radius of M^{2+} is to that of Li^{+}, as well as on the synthesis protocol. The metal occupancies determined at 20 K were used to analyze the NPD data collected at 3 K. The final Rietveld plot and crystallographic information for $P2_1/n$ Li_2MnSiO_4 at 20 K are presented in Figure S3 and Table S5, respectively.

Examination of the NPD data collected at 3 K revealed additional intensity due to long-range magnetic ordering. All the diffraction peaks with magnetic contributions could be indexed by the unit cell with doubled a- and c-parameters, i.e., with the propagation vector k = (1/2, 0, 1/2). For the general 4e(x, y, z) Wyckoff site of the $P2_1/n$ space group, the magnetic representation decomposes in terms of four one-dimensional irreducible representations (IR) as $\Gamma_{mag}(4e) = 3\Gamma1 + 3\Gamma2 + 3\Gamma3 + 3\Gamma4$. The associated basis vectors are listed in Table S6. The best agreement between experimental and calculated powder diffraction patterns was obtained for the Γ1 representation. Simultaneous refinement of all three basis vector coefficients revealed that the value corresponding to the F_y mode oscillated around zero, within a standard deviation, which is consistent with the absence of an FM signal in the magnetization data (Figure S1). Therefore, this coefficient was fixed to zero and only those corresponding to the G_x and G_z modes were refined. The final Rietveld plot and crystallographic information are presented in Figure 5 and Table S7.

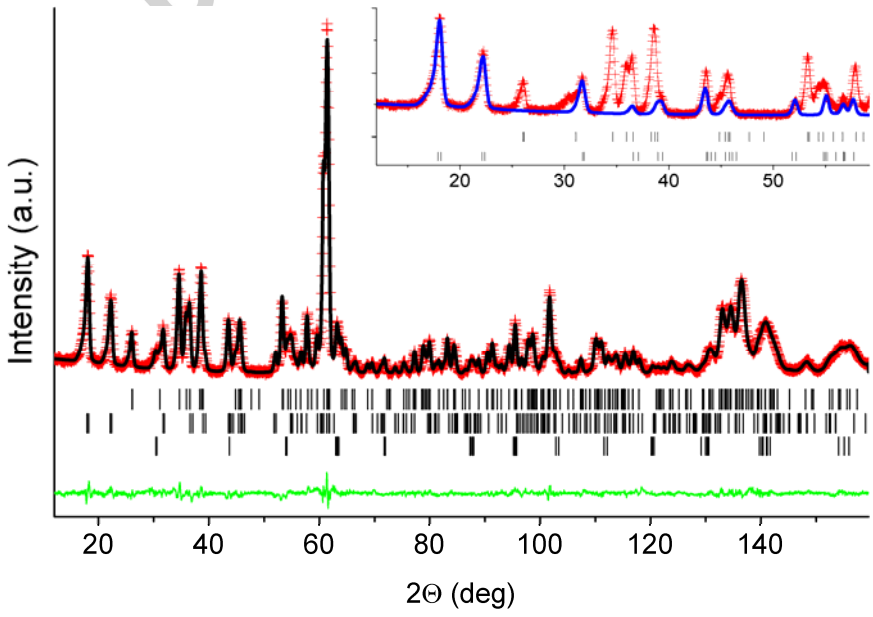

Figure 5. The Rietveld plot for Li_2MnSiO_4 refined against NPD data collected at 3 K. The red crosses and black and green solid lines indicate the observed and calculated patterns and their difference, respectively. The tick marks from top to bottom indicate the position of the diffraction peaks of the nuclear structure of Li_2MnSiO_4, the magnetic structure of Li_2MnSiO_4, and Li_2SiO_3, respectively. R_p = 3.18%, R_{wp} = 4.11%, $R_F(Li_2MnSiO_4)$ = 1.82%, R_{mag} = 4.21%. The blue curve in the inset shows the magnetic contribution only.

Like the cobalt analog, Li_2MnSiO_4 adopts a collinear AFM structure (Figure 6). The magnetic moments are oblique to the distorted close-packing oxygen layers (the angle to the c-axis is 31.6°) with components along a-, b-, and c-axes of 2.40(4), 0, and 3.91(4) μ_B respectively, yielding a total magnetic moment of 4.6 μ_B/Mn. This slightly reduced value compared to that expected for high-spin S=5/2 d^5 Mn^{2+} is most likely related to the disruption of local exchange pathways by the ~10% of Li^+ present on Mn^{2+} sites (Table S5). The magnetic structure is further discussed below in comparison to that of Li_2CoSiO_4.

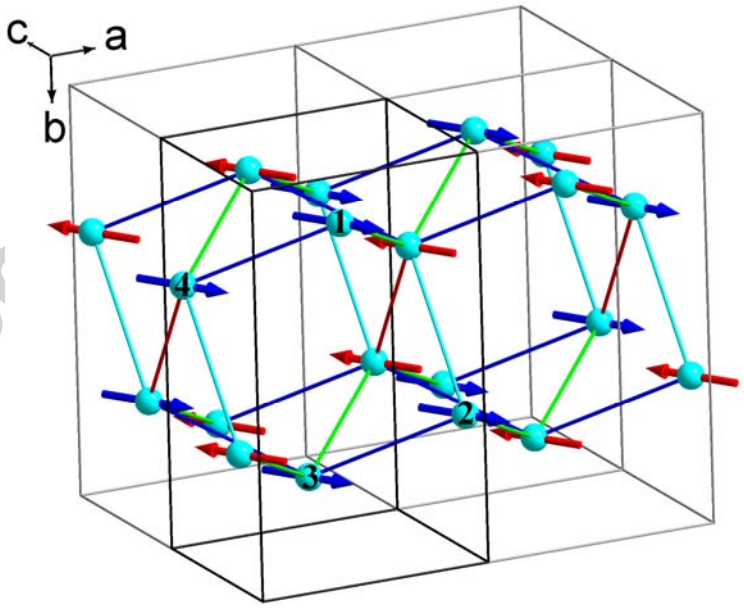

Figure 6. General view of Li_2MnSiO_4 magnetic structure (non-magnetic atoms omitted). Nuclear and magnetic unit cells are shown with black and gray lines, respectively. The four inequivalent sets of Mn-Mn dis-

tances (4.14 Å, 4.41 Å, 4.48 Å, and 4.74 Å) are shown with red, green, blue, and cyan lines, respectively. The numbers show the atom sequence used for further analysis of the magnetic phase diagram (see text).

Comparison of β_I-Li_2CoSiO_4 and γ_0-Li_2MnSiO_4 magnetic structure

As discussed above and illustrated in Fig. 1, $Pbn2_1$ β_I-Li_2CoSiO_4 and $P2_1/n$ γ_0-Li_2MnSiO_4 crystallize in different structure types with different patterns of cation distribution over the tetrahedral interstitial sites of close-packed oxygen arrays. When the structures are considered in terms of nearest-neighbor bonds and coordination polyhedra, they have different local arrangements of the silicate groups that bridge magnetic atom sites (Fig. 7): in Li_2CoSiO_4 all the silicate tetrahedra point in the same direction; while in Li_2MnSiO_4 they adopt an up/down pattern.

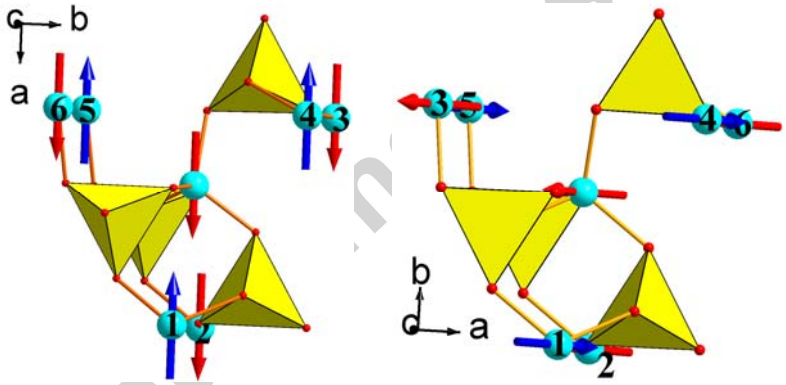

Figure 7. Local arrangement of silicate groups (yellow tetrahedra) connecting magnetic atom sites in Li_2CoSiO_4 (left) and Li_2MnSiO_4 (right). Numbers are further used in Fig. 10.

However, examination of the magnetic sublattices in the two materials reveals that despite the different orientations of cation polyhedra, the arrays of magnetic metals are very similar, albeit slightly distorted in the monoclinic Li_2MnSiO_4 (Fig. 8). Furthermore, although the moments have different orientation with respect to oxygen close packed layers (parallel in Li_2CoSiO_4 and oblique in Li_2MnSiO_4), the magnetic ordering scheme is the same (Fig. 7, 8).

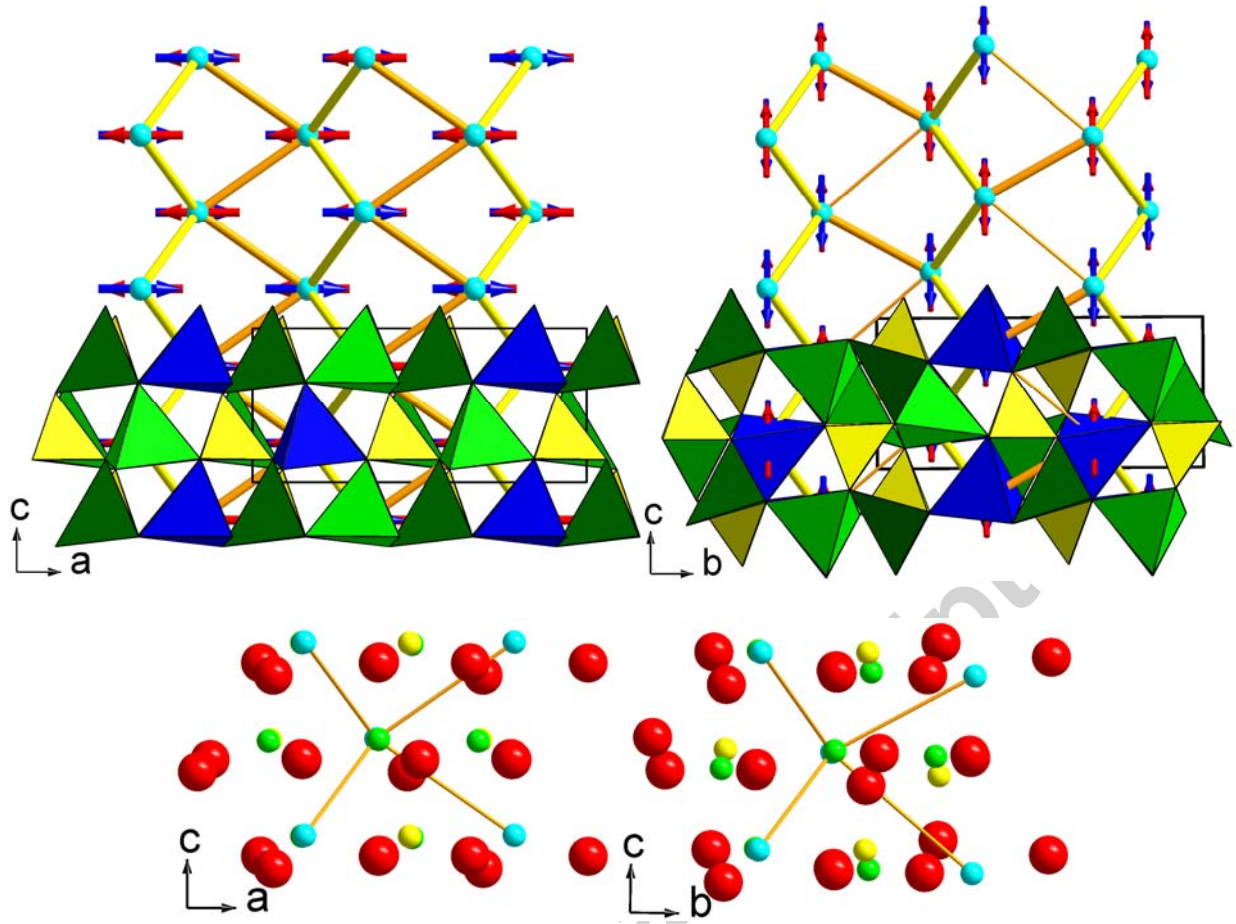

Figure 8. Magnetic sublattices of Li_2CoSiO_4 (left) and Li_2MnSiO_4 (right) with respect to their crystal structures. Metal color scheme is the same as in Fig. 1. The bottom row illustrates that the rearrangement of cations from the case where tetrahedra point only along c-axis (left) to the case where they point down (right) only very weakly affects the magnetic metal array; oxygen atoms are shown as red spheres.

There are several different ways in which the magnetic structure of these materials can be described. One, hinted at by the propagation vectors, is as AFM zigzag chains running along the (011) and (101) direction in Li_2CoSiO_4 and Li_2MnSiO_4 respectively, coupled ferromagnetically in the (01-1) and (10-1) directions respectively (Fig. 9). Alternatively, it can be described as corrugated FM layers of hexagons coupled antiferromagnetically (Fig. 9).

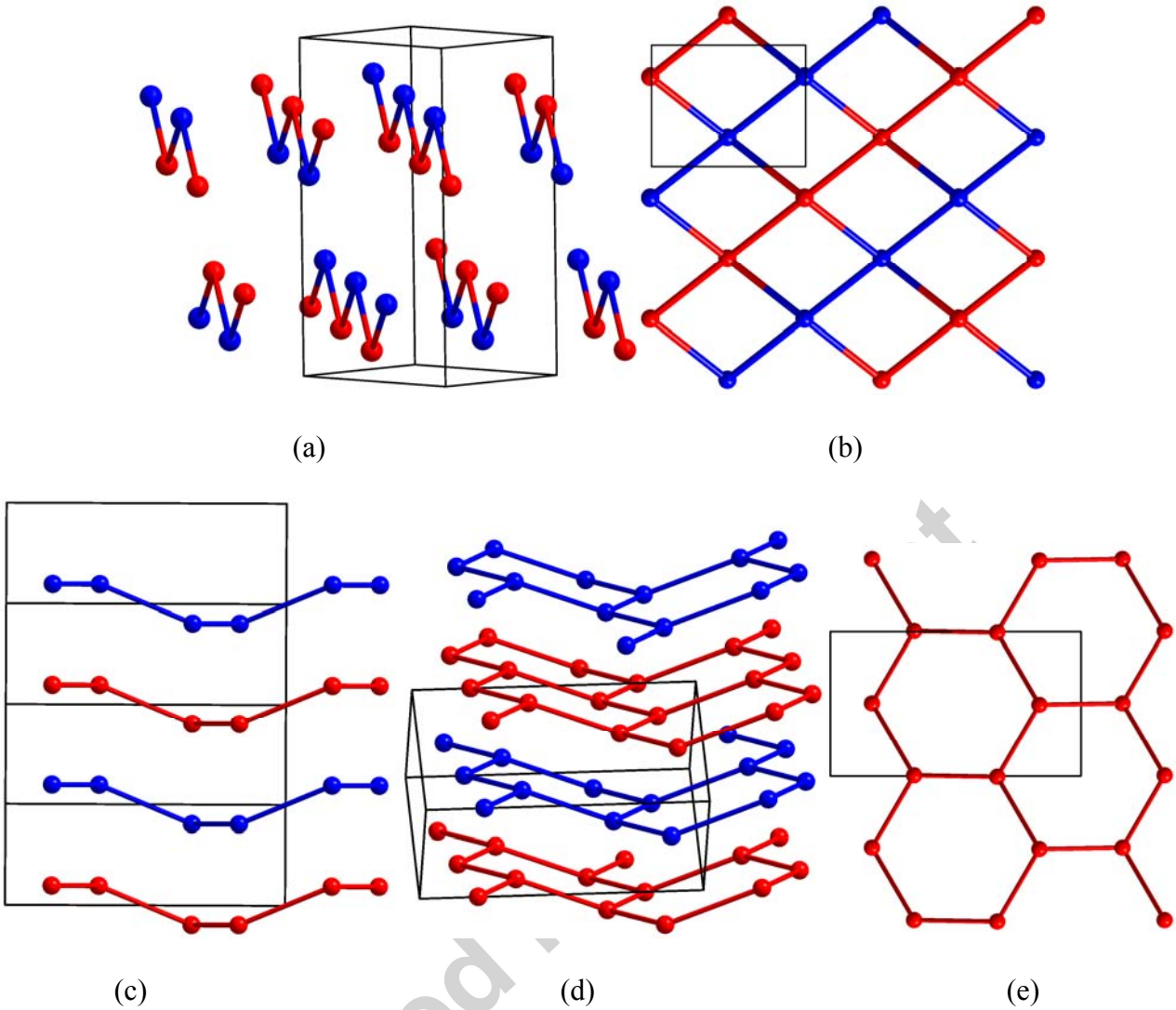

Figure 9. (a,b) AFM zigzag chains running along (011) and (101) in Li_2CoSiO_4 and Li_2MnSiO_4, respectively; (c-d) corrugated FM layers of hexagons stacked perpendicular to (011) and (101) in Li_2CoSiO_4 and Li_2MnSiO_4, respectively; (e) projection of a single corrugated layer perpendicular to c-axis in both structures (note that the layer is not perpendicular to c-axis).

In order to explain both why these two materials adopt the same type of magnetic ordering, we have examined the topology and geometry of the magnetic exchange pathways. In both materials the magnetic metal tetrahedra [MO_4] are connected via bridging [SiO_4] groups, such that magnetic interactions with their six nearest neighbors occur only via super-super-exchange (Fig. 7). When M-O-O-M contacts are presented as graphs it becomes obvious that the materials have an identical pathway topology (Fig. 10).

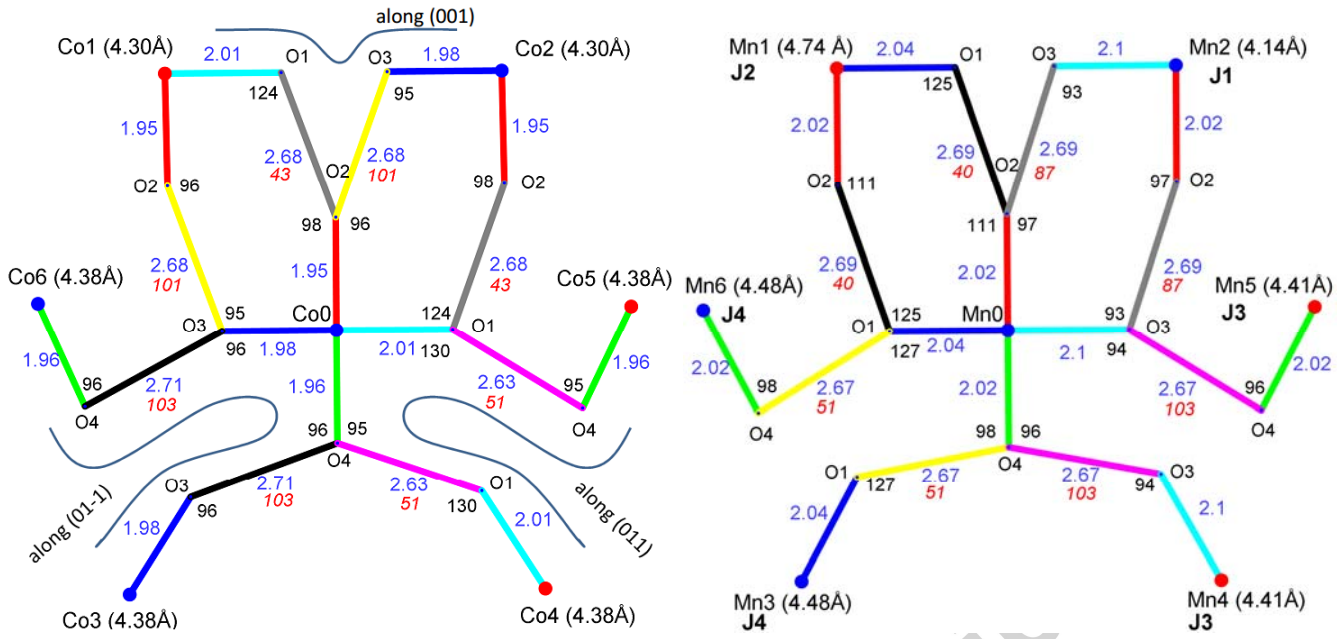

Figure 10. Topology and geometry of magnetic exchange pathways in Li_2CoSiO_4 (left) and Li_2MnSiO_4 (right) between a magnetic atom and six nearest neighbors. Equivalent interatomic distances in each structure are shown in the same color. Distances, M-O-O angles, and M-O-O-M torsion angles are included in blue, black, and red fonts, respectively. Values in parentheses indicate metal-metal distances. Blue and red coloring of the vertices indicate FM and AFM coupling, respectively. Atom numbering is the same as in Fig. 6.

Both materials have rather low symmetry with a number of inequivalent interatomic distances and angles. Each magnetic atom has two double and four single M-O-O-M contacts (Fig. 10). In Li_2CoSiO_4, six metal-metal distances form two sets (2x4.30 Å and 4x4.38 Å), while in Li_2MnSiO_4 the monoclinic distortion results in four inequivalent distances (4.14 Å, 2x4.41 Å, 2x4.48 Å, and 4.74 Å). Some of the M-O-O' angles are in the range 120-130° and some of the M-O-O'-M' torsion angles are rather twisted (Fig. 10) so that the type of resulting magnetic coupling between M and M' is difficult to predict based on Goodenough-Kanamori rules [21, 22]. However, a magnetic phase diagram in terms of relative strength of classical isotropic Heisenberg exchange interactions (a behavior often found for high-spin d^5 L=0 Mn^{2+}) calculated using the ENERMAG program ([23] and references therein) correctly predicts stability of the experimentally

observed magnetic structure for Li_2MnSiO_4 (Fig. 11). Regardless of whether J_4 corresponding to the longest Mn-Mn distance, 4.74 Å, (Fig. 9) is weakly positive or negative, the experimental phase is stable for the combination of $J_1>0$, $J_3<0$, and $J_4>0$ (Fig. 11). The negative J_3 and positive J_1/J_4 define the AFM zigzag chains and the FM hexagons shown in Fig. 9, respectively.

For Li_2CoSiO_4, however, consideration of only isotropic exchange with six nearest neighbors is not sufficient to interpret the magnetic structure. As can be seen in Fig. 10, the Co1 and Co2 atoms have identical connectivity with the central atom Co0, while being AFM and FM coupled, respectively. This suggests that the experimentally observed magnetic structure is stabilized by next-nearest-neighbor (NNN) interactions (structure examination reveals that these are primarily AFM) and/or magnetocrystalline anisotropy often playing significant role in Co^{2+} materials, although detailed energy mapping analysis using ab initio calculations [24] would be required to confirm that.

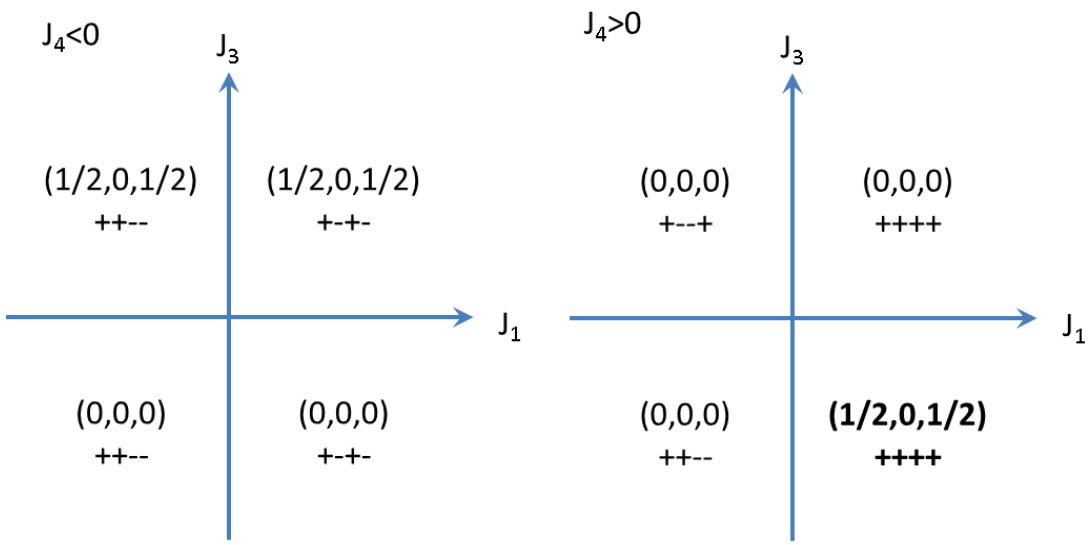

Figure 11. Magnetic phase diagram for Li_2MnSiO_4 in terms of the relative strength of isotropic exchange interactions between a magnetic atom and its six nearest neighbors. The + and - symbols indicate relative "up" and "down" moment direction, respectively. The numbering scheme of J_{ij} and the atom sequence are the same as for Fig. 10 and Fig. 6, respectively. The field of the experimentally observed magnetic structure is indicated in bold font.

CONCLUSIONS

Although $Pbn2_1(\equiv Pna2_1)$ Li_2CoSiO_4 and $P2_1/n$ Li_2MnSiO_4 crystallize in distinct crystal structure types with different ordering of cation tetrahedra, this does not change the topology of M-O-O'-M' super-super-exchange pathways. Magnetometry and neutron powder diffraction data show that both materials adopt magnetic structure of the same type. Calculations of a magnetic phase diagram for Li_2MnSiO_4 in terms of the relative strength of isotropic exchange between Mn^{2+} and its 6 nearest neighbors correctly predicts the stability of the experimentally observed magnetic structure. However, this analysis fails for Li_2CoSiO_4, which will require a more sophisticated theoretical analysis taking into account next-nearest-neighbor interactions and weaker contributions, e.g., spin-orbit coupling. Li_2CoSiO_4 is thus an excellent example of a key practical motivation for solving the ordered magnetic ground states of these lithium-ion battery cathode materials, which is to allow for experimental verification of *ab initio* calculations. Any such calculations for $Pbn2_1(\equiv Pna2_1)$ Li_2CoSiO_4 and $P2_1/n$ Li_2MnSiO_4 that fail to reproduce the low-temperature magnetic ground states reported here will be open to the criticism that they may have not reached a sufficient level of precision to quantitatively predict their electronic and electrochemical properties at technologically relevant temperatures.

ASSOCIATED CONTENT

Supporting Information

Rietveld plots for NPD data collected at 20 K, tables with crystallographic information at 20 K and 3 K and representational analysis for $Pna2_1$ and $P2_1/n$ space groups. This material is available free of charge via the Internet at http://pubs.acs.org.

AUTHOR INFORMATION

Corresponding Author

* Maxim.Avdeev@ansto.gov.au

Author Contributions

All authors have given approval to the final version of the manuscript.

Notes

The authors declare no competing financial interests.

ACKNOWLEDGMENT

C.D.L. acknowledges the financial support from the Australian Research Council (DP110102662). Z.M. acknowledges financial support from Ministry of Higher Education Malaysia and Universiti Teknologi MARA.

ABBREVIATIONS

FM, ferromagnetic; AFM, antiferromagnetic; NPD, neutron powder diffraction; FC, field cooled; ZFC, zero-field cooled.

REFERENCES

[1] C. Masquelier, L. Croguennec, *Chemical reviews* 113 (2013) 6552–6591.
[2] M. Armand, C. Michot, N. Ravet, M. Simoneau, P. Hovington, US, 2000.
[3] A. West, F. Glasser, *Journal of Solid State Chemistry* 4 (1972) 20-28.
[4] A. West, F. Glasser, *Journal of Materials Science* 5 (1970) 676-688.
[5] W. Baur, T. McLarnan, *Journal of Solid State Chemistry* 42 (1982) 300-321.
[6] A. Saracibar, A. Van der Ven, M.E. Arroyo-de Dompablo, *Chemistry of Materials* 24 (2012) 495-503.
[7] R. Gummow, Y. He, *Journal of Power Sources* 253 (2014) 315-331.
[8] K. Zaghib, A. Ait Salah, N. Ravet, A. Mauger, F. Gendron, C. Julien, *Journal of Power Sources* 160 (2006) 1381-1386.
[9] M. Bini, S. Ferrari, C. Ferrara, M.C. Mozzati, D. Capsoni, A.J. Pell, G. Pintacuda, P. Canton, P. Mustarelli, *Scientific reports* 3 (2013).
[10] I. Belharouak, A. Abouimrane, K. Amine, *The Journal of Physical Chemistry C* 113 (2009) 20733-20737.
[11] M.M. Kalantarian, S. Asgari, P. Mustarelli, *Journal of Materials Chemistry A* 1 (2013) 2847-2855.
[12] M. Ramzan, S. Lebegue, R. Ahuja, *Physical Review B* 82 (2010).
[13] K.-F. Hesse, *Acta Crystallographica Section B: Structural Crystallography and Crystal Chemistry* 33 (1977) 901-902.
[14] V.V. Politaev, A.A. Petrenko, V.B. Nalbandyan, B.S. Medvedev, E.S. Shvetsova, *Journal of Solid State Chemistry* 180 (2007) 1045-1050.
[15] J. Rodríguez-Carvajal, *Physica B: Condensed Matter* 192 (1993) 55-69.
[16] R.L. Carlin, *Magnetochemistry*. Springer Berlin, 1986.
[17] H. Yamaguchi, K. Akatsuka, M. Setoguchi, Y. Takaki, *Acta Crystallographica Section B: Structural Crystallography and Crystal Chemistry* 35 (1979) 2680-2682.
[18] A.R. Armstrong, C. Lyness, M. Ménétrier, P.G. Bruce, *Chemistry of Materials* 22 (2010) 1892-1900.
[19] W. Hamilton, *Acta Crystallographica* 18 (1965) 502-510.
[20] M. Viola, M. Martínez-Lope, J. Alonso, J. Martínez, J. De Paoli, S. Pagola, J. Pedregosa, M. Fernández-Díaz, R. Carbonio, *Chemistry of materials* 15 (2003) 1655-1663.
[21] J.B. Goodenough, *Magnetism and the chemical bond*. Interscience Publishers New York, 1963.
[22] J. Kanamori, *Journal of Physics and Chemistry of Solids* 10 (1959) 87-98.
[23] N. El Khayati, R.C. El Moursli, J. Rodríguez-Carvajal, G. André, N. Blanchard, F. Bourée, G. Collin, T. Roisnel, *The European Physical Journal B-Condensed Matter and Complex Systems* 22 (2001) 429-442.
[24] H. Xiang, C. Lee, H.-J. Koo, X. Gong, M.-H. Whangbo, *Dalton Transactions* 42 (2013) 823-853.

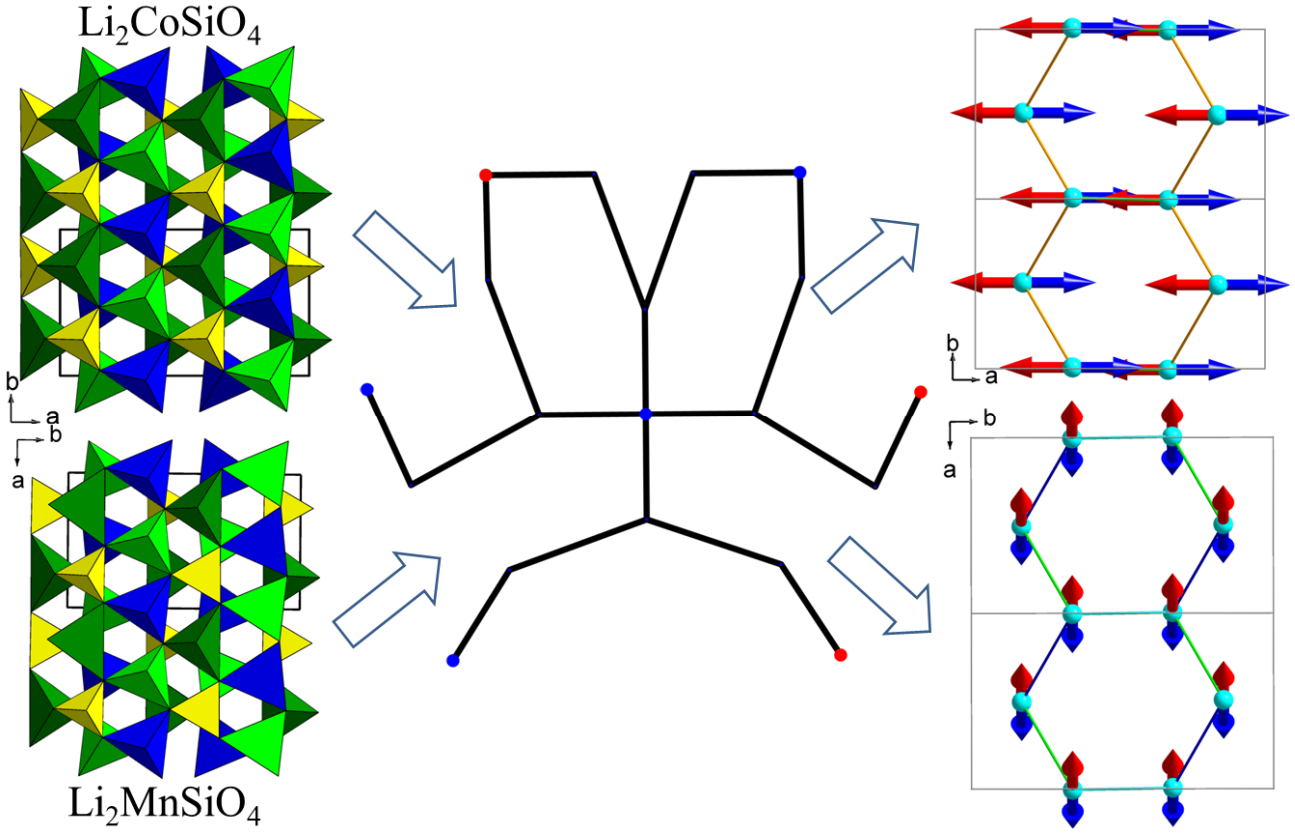

TOC Figure

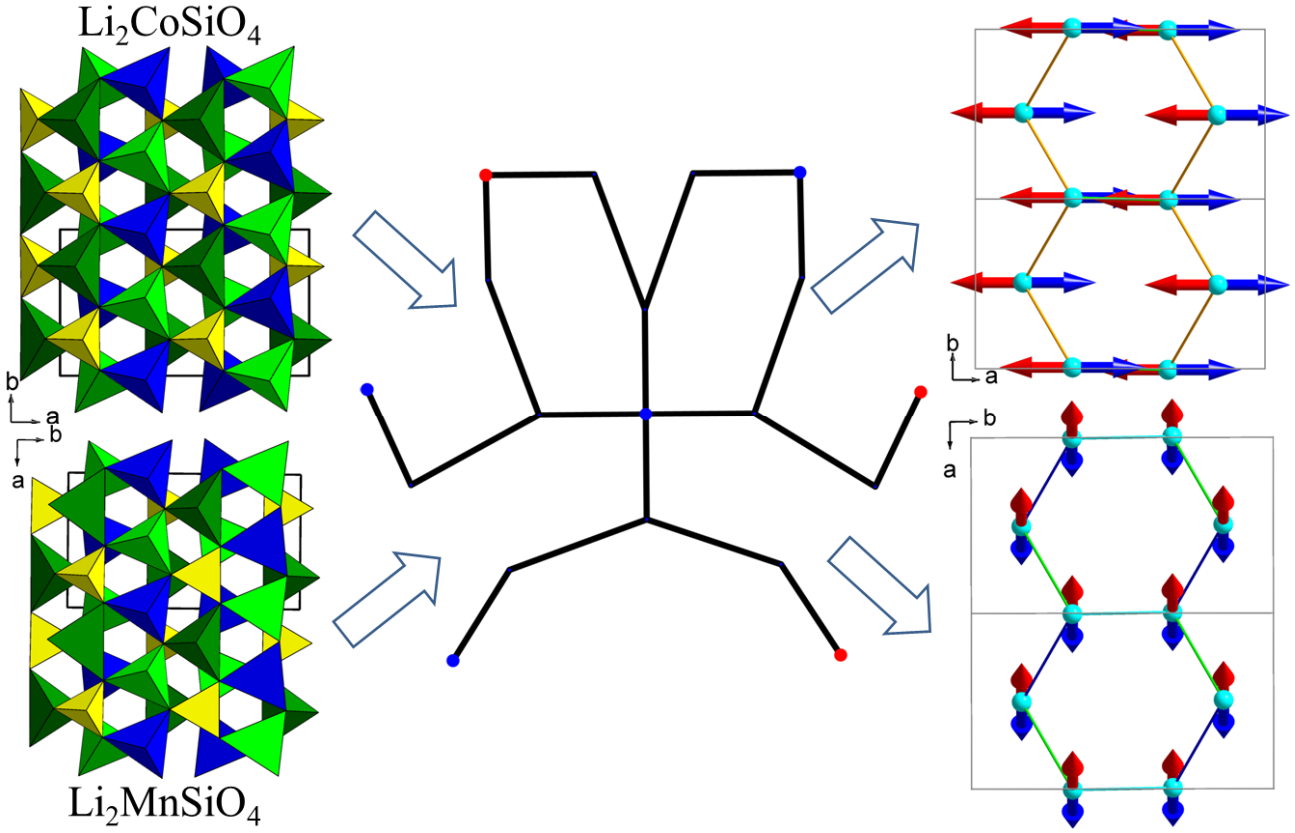

TOC Figure

TOC Figure caption:

Despite the different crystal structures β_I-Li_2CoSiO_4 and γ_0-Li_2MnSiO_4 have similar magnetic topology and as a result adopt magnetic structure of the same type.

Highlights:

- Magnetic structures of Li_2CoSiO_4 and Li_2MnSiO_4 were studied for the first time
- Both materials antiferromagnetically order around 12-14 K
- Despite different crystal structure magnetic structures are of the same type
- The fact is attributed to similar topology of magnetic interactions